



Visible light photoactivity of the Cu doped $\text{TiO}_2/\text{Yb}_2\text{O}_3$ nanocomposite for degradation of acid red 88 solution

Sarvin Mohammadi-Aghdam¹ · Zirar M. Mizwari^{2,3} · Hossein Khojasteh⁴

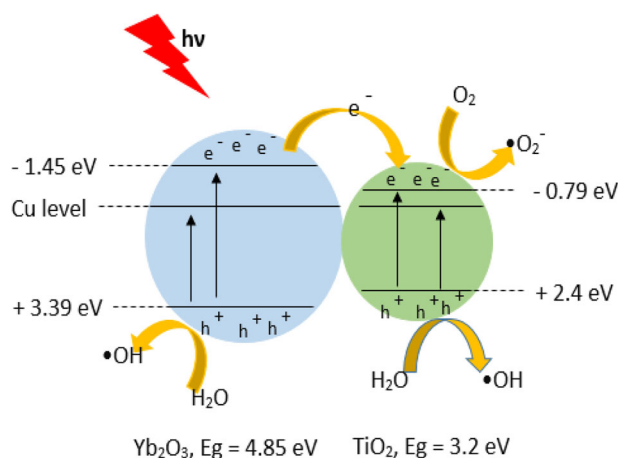
Received: 25 January 2023 / Accepted: 19 June 2023 / Published online: 24 July 2023

© The Author(s), under exclusive licence to Springer Science+Business Media, LLC, part of Springer Nature 2023

Abstract

The highly efficient Cu doped $\text{TiO}_2/\text{Yb}_2\text{O}_3$ (CTYO) photoactive nanocomposite were prepared by simple and straight sol-gel method. The structural, morphological and other properties of the prepared nanocomposite were studied. X-ray diffraction analysis revealed the existence of both Yb_2O_3 and TiO_2 phases in crystalline structure of CTYO. UV-Vis diffuse reflectance spectroscopy confirmed the great potential of the prepared samples as the efficient visible light photocatalyst. The photoactivity of the prepared samples were evaluated using degradation of acid red 88 solution (AR88) under visible light irradiation. The 92.5% of the AR88 in solution was degraded after the 180 min illumination over CTYO photocatalyst. The degradation efficiency was studied under different pH of AR88 solution and amounts of the loaded photocatalyst. The stability and recyclability of the prepared photocatalyst were studied under 8 reaction cycles which revealed the superiority of CTYO as the visible light photocatalyst.

Graphical Abstract



Keywords Cu-doped · $\text{TiO}_2/\text{Yb}_2\text{O}_3$ · Nanocomposite · Photocatalyst · Visible light · AR88 solution

✉ Sarvin Mohammadi-Aghdam
Sarvin.s108@pnu.ac.ir

¹ Department of Chemistry, Payame Noor University, Tehran, Iran

² Department of Medical Laboratory Technology, Shaqlawa Technical College, Erbil Polytechnic University, Erbil, Iraq

³ Rwandz Private Technical Institute, Erbil, Iraq

⁴ Department of Nanotechnology, Scientific Research Center, Soran University, Soran-Erbil, Kurdistan Region, Iraq

Highlights

- Cu doped TiO₂/Yb₂O₃ nanocomposite was prepared using simple Sol-Gel method.
- Prepared nanocomposite has an excellent visible light photocatalytic activity.
- Prepared nanocomposite has a superior stability under successive reaction cycles.

1 Introduction

In recent years, scientific research has been focused on developing a possible and efficient approach to solving the environmental crisis relating to increasing population growth, industrial and agricultural activities [1, 2]. Contamination of oceans and sweet-water resources poses a serious threat not only to human health but also to life on the earth [3, 4]. In this regard, the photocatalytic process is the most promising method for treatment of wastewater, due to the possibility of solar energy harvesting and environmentally friendly nature [5, 6].

The photocatalyst material is activated by absorbing photons with energy equal to the band gap energy of semiconductor, thereby generating charge carriers (electrons and holes e^-/h^+) which produce extremely reactive radicals toward oxidation of the organic pollutants in aqueous media [1]. Titanium dioxide (TiO₂) is a common photocatalyst material which is widely used in the photocatalytic process. However, low quantum efficiency of TiO₂ caused by the wide range band-gap of TiO₂ (3.0–3.2 eV) considerably restricts the large scale application of TiO₂ [6, 7]. Moreover, fast recombination rate of the charge carriers is another limitation of TiO₂ photocatalyst.

Therefore, research on the photocatalytic treatment of wastewater has been devoted to the more efficient photocatalyst material. Mixed metal oxides are an appropriate alternative to common photocatalyst materials, due to having striking electrical, electronic, optical and other physiochemical properties [8–10].

In this regard, the heterostructure composites are an important class of the photocatalyst materials which are composed of two or more different semiconductors. The Heterostructure photocatalyst could substantially promotes separation of charges and reduces the recombination rate of electrons and holes.

Rare earth metal oxide are good materials to make the efficient heterostructure photocatalyst, which is due to partially occupied 4f and empty 5d orbitals in the rare earth metals [11]. The rare earth metal oxide could well participates to reduce the recombination rates of charges in the heterostructure photocatalyst [12]. Recently, the heterostructure composites based on rare earth metal oxide have been extensively studied because of their excellent photocatalytic potential.

For instance, Janani et al. prepared ZnO-Al₂O₃-CeO₂-Ce₂O₃ mixed metal oxides as an efficient photocatalyst materials for degradation of methyl orange under UV irradiation [13]. Vignesh et al. prepared g-C₃N₄-Ce₂O₃-CuO ternary photocatalyst for visible light degradation of methyl yellow and methylene blue [14]. Mohamed et al. reported Nd₂O₃ modified ZnO nanoparticles for degradation of tetracycline under visible light irradiation [15]. Basaleh et al. used a novel CdS/Gd₂O₃ nanocomposite for photoreduction of Cr (VI) [16]. In addition, Munawar et al. prepared ZnO-CeO₂-Yb₂O₃ heterostructured nanocomposite as efficient photocatalyst and antibacterial material [17]. Modwi et al. used a Yb₂O₃/ZnO nanocomposite for degradation of congo red under visible light [18].

Doping with metal ions is another effective way to enhance the photocatalytic activity of photocatalyst and extent its optical response into visible light irradiation. In this regard, Liyanaarachchi et al. prepared Cu doped TiO₂/g-C₃N₄ photocatalyst for degradation of methylene blue under visible light irradiation [19]. Also, Yuzer et al. studied the photocatalytic, self-cleaning and antibacterial properties of Cu doped TiO₂ [20].

In this study, we prepared Cu doped TiO₂/Yb₂O₃ nanocomposite using facile and cost-effective sol-gel method. The photocatalytic properties of the prepared nanocomposites were studied for degradation of acid red 88 (AR88) solution under visible light irradiation. The effect of different concentrations of Cu doped into CTYO structure was studied on the structural, optical and photocatalytic properties of the prepared CTYO nanocomposite.

2 Experimental

2.1 Sol-Gel preparation of CTYO nanoparticles

First, 1 mmol of tetrabutyl orthotitanate (TBOT) was dissolved into 40 mL solution of polypropylene glycol (PPG) (5 mL) and ethanol (35 mL). Then, 1 mmol of Yb(NO₃)₃·5H₂O and certain amount of Cu(NO₃)₂·3H₂O (0.0, 0.02 and 0.04 mmol) were added to the above solution. The solution were stirred for 60 min to form a light blue homogeneous mixture of precursors. The gel was dried overnight at 90 °C. The dried gel was calcined at 600 °C for 5 h under air atmosphere to form light gray solid. The same procedure was followed to prepare the pure TiO₂ without addition of any Yb and Cu precursors.

2.2 Characterization

The crystalline structure of the prepared samples (pure TiO₂ and CTYO nanocomposites) were studied using X-ray diffraction patterns (XRD) (Philips X'pert Pro MPD, Cu $k\alpha = 1.54 \text{ \AA}$). The morphology and surface properties of the prepared CTYO nanocomposites were studied by field emission scanning electron microscopy (FE-SEM) images (TESCAN Mira3). The composition of the prepared sample was investigated using energy dispersive X-ray (EDX) spectroscopy (TESCAN Mira3). The chemical groups of the prepared sample was recorded using Fourier transform infrared spectroscopy (FT-IR) (Shimadzu Varian 4300 spectrometer). The optical properties of the prepared samples were studied using photoluminescence spectroscopy (PL) (Varian Cary Eclipse) and UV-Vis diffuse reflectance spectroscopy (DRS) (Shimadzu UV-670).

2.3 Photocatalytic study of CTYO

The photocatalytic efficiency of the prepared CTYO photocatalyst was studied using visible light degradation of acid red 88 (AR88) solution. The photocatalytic experiments were conducted by constant concentration of AR88 solution (20 mg L⁻¹). The metal halide OSRAM lamp (HQIBT 400 W/D/DE40FLH1) was used as the visible light source and the distance between light source and reaction solution was kept constant to 30 cm. Before the illumination, the reaction solution was kept in darkness to achieve adsorption/desorption equilibrium between dye molecules and the photocatalyst particles. The photocatalytic degradation of AR88 was monitored at a constant time interval (30 min) of visible light illumination. The photocatalyst particles were separated from dye solution using centrifugation at 6000 rpm for 10 min. The concentration of treated AR88 solution was determined using UV-Vis spectrophotometer at $\lambda_{\max} = 506 \text{ nm}$

3 Results and discussion

3.1 Characterization of Cu doped TiO₂/Yb₂O₃ (CTYO) nanocomposite

The phase structure and crystallinity of the prepared CTYO nanocomposites were studied using XRD analysis, as shown in Fig. 1. As can be seen, the CTYO nanocomposites show the diffraction peaks at $2\theta = 20.94^\circ, 25.38^\circ, 29.70^\circ, 34.39^\circ, 40.55^\circ, 44.27^\circ, 48.11^\circ, 49.45^\circ, 53.88^\circ, 55.11^\circ, 58.71^\circ, 60.04^\circ, 61.52^\circ$ and 62.89° .

Undeniably, the diffraction peaks at $2\theta = 20.94^\circ, 29.70^\circ, 34.39^\circ, 40.55^\circ, 44.27^\circ, 49.45^\circ, 58.71^\circ$ and $60.04^\circ, 61.52^\circ$ (marked with ♣) are truly attributed to the cubic phase of the Yb₂O₃ (06-0371 JCPDS file no). In addition, the

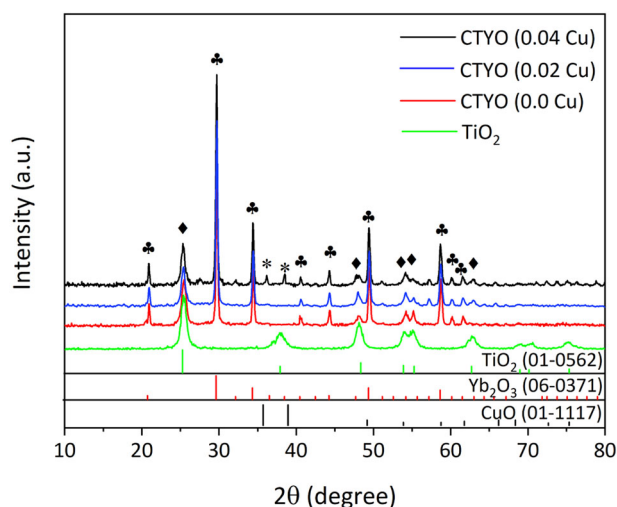


Fig. 1 XRD patterns for the prepared CTYO nanocomposites

diffraction planes of the anatase TiO₂ (01-0562 JCPDS file no.) are appeared at $2\theta = 25.38^\circ, 48.11^\circ, 53.88^\circ, 55.11^\circ$, and 62.89° (marked with ♦). Clearly, for the sample prepared with 0.02 mmol Cu dopant, there are no diffraction peak for CuO phase which revealed that the Cu atoms are well doped into the CTYO crystalline structure. However, two diffraction peaks at 35.84° and 38.44° (marked with *) are appeared at the exceeded concentration of Cu dopant which are related to CuO phase (01-1117 JCPDS file no.). Owing to the existence of these two characteristic diffraction peaks, it is clear that the most of Cu ions are in +2 oxidation state and form CuO phase. The CuO phase is dissolved in TiO₂/Yb₂O₃ matrix.

The average crystallite size of the prepared sample was calculated using Scherrer equation (Eq. 1), employing the peak at $2\theta = 29.70^\circ$:

$$D = \frac{k\lambda}{\beta \cos \theta} \quad (1)$$

where D is the average crystallite size, λ is the X-ray wavelength, β is the full width of diffraction peak at the half maximum (FWHM), k is a shape factor and θ is the diffraction peak angle. The average crystallite size of the prepared CTYO nanocomposites with different concentration of Cu dopant (0.0, 0.02 and 0.04) was calculated to be 17.4 nm, 18.2 nm and 25.3 nm, respectively.

Figure 2a, b show the FE-SEM images for the prepared CTYO nanocomposite (Cu dopant concentration = 0.02 mmol) which demonstrate that the prepared CTYO have uniformly nanosphere morphology with the average size below 50 nm. In addition, due to heat treatment of prepared sample, slightly agglomerated particles is observed in FE-SEM images.

The composition and elemental distribution of the prepared CTYO nanocomposite (Cu dopant concentration =

Fig. 2 FESEM images for the prepared CTYO nanocomposite (Cu dopant concentration = 0.02 mmol) at different magnifications. 500 nm (a) and 200 nm (b)

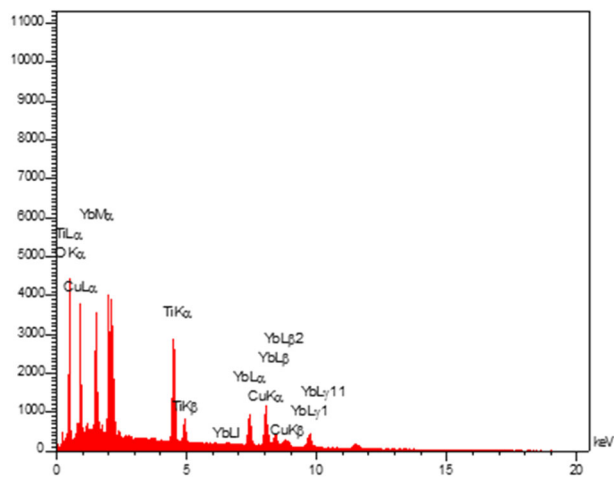
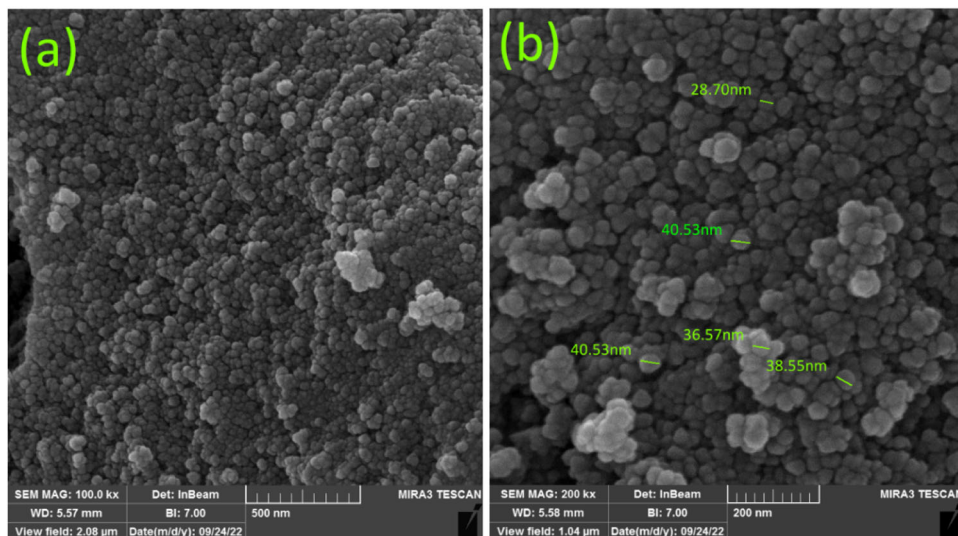


Fig. 3 EDX spectra for the prepared CTYO nanocomposite (Cu dopant concentration = 0.02 mmol)

0.02 mmol) were studied using EDX spectroscopy, as shown in Fig. 3. In addition, the elemental microanalysis results reveal the relative amount (wt%) of each components is Ti (11.38%), Yb (70.19%), Cu (0.19%) and O (18.24%).

The chemical functional groups on the surface of the CTYO nanocomposite (Cu dopant concentration = 0.02 mmol) were determined using Ft-IR analysis which shown in Fig. 4. The FT-IR spectrum for the prepared CTYO nanocomposite represents a broad absorption peak centered at 3492 cm^{-1} which is assigned to the stretching vibration of O–H groups. In addition, the bending vibration of O–H is clearly seen at 1609 cm^{-1} . Due to the exposure to the ambient atmosphere, Yb-carbonate groups form on the surface of nanoparticles. The surface carbonated groups are clearly identified at the two absorption peaks at 1467 and 1344 cm^{-1} [21]. Moreover, there is a strong absorption peak

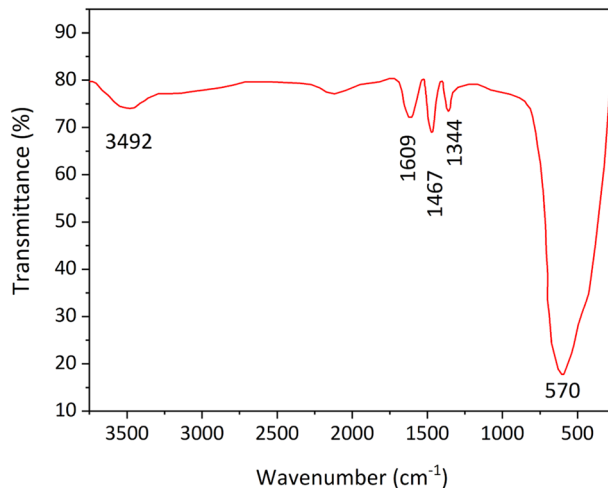


Fig. 4 FT-IR spectra for the prepared CTYO nanocomposite (Cu dopant concentration = 0.02 mmol)

at 570 cm^{-1} which is truly attributed to the metal-oxygen bonds [22].

The light absorption ability and optical properties of the prepared samples were studied using UV-Vis spectroscopy. Figure 5 shows the DRS spectra for the samples prepared with different concentration of Cu dopant at the wavelength range of 250–700 nm. As can be seen, the different concentrations of Cu dopant significantly alter the visible light absorption properties of the CTYO. The sample prepared using 0.02 mmol of Cu dopant has the increased light absorption at both visible and UV region. However, the exceeded content of Cu dopant (0.04 mmol) led to a slightly decrease in the UV-Vis light absorption. The absorption peak around 350 nm belongs to the $\text{TiO}_2/\text{Yb}_2\text{O}_3$ matrix which is shifted to the longer wavelength as concentration of dopant increases. Besides, a shoulder-like peak at range 280–310 nm could be assigned to the ligand to metal charge

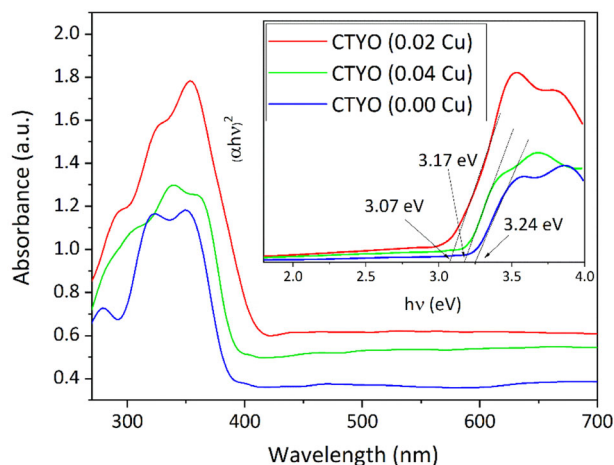


Fig. 5 DRS spectra and inset: plot of $(\alpha h\nu)^2$ vs. $h\nu$ for the prepared CTYO with different concentrations of Cu dopant

transfer transition ($O^{2-}(2p) \rightarrow Cu^{2+}(3d)$) [23]. Clearly, the absorption edge is shifted to longer wavelength with increasing the dopant concentration.

In order to determine the variations in the band-gap energy depending on the different concentrations of Cu dopant, the Kubelka-Munk method [24] was used to calculate the band gap of the prepared CTYO nanocomposites. As shown in inset to Fig. 5, by plotting $(\alpha h\nu)^2$ vs. $h\nu$, the band gap of the prepared samples were obtained with extrapolation of the linear part of the spectra to the horizontal axis. As expected, the sample containing 0.02 mmol of Cu dopant has the lowest band-gap of the 3.07 and the highest band-gap of the 3.24 eV is assigned to the sample prepared without any Cu dopant. Also, the 0.04-Cu doped TiO_2/Yb_2O_3 nanocomposite has the band-gap of the 3.17.

The photo-generated electrons and holes during the photocatalyst illumination have a short lifetime (few ns). The photo-generated electrons are in the excited state which could either decay radiatively or migrate to the surface of the photocatalyst to participate in the photocatalytic reaction [25].

Figure 6 shows the PL spectra for the CTYO nanocomposites with different concentration of Cu dopant (0.0, 0.02 and 0.04 mmol) at constant excitation wavelength of 300 nm. For this purpose, 0.01 g of as-prepared CTYO nanocomposites were dispersed into 50 mL of deionized water using ultrasonication bath for 15 min. Then, the solution of dispersed nanocomposites powders were studied by PL spectroscopy. Obviously, the PL intensity is affected by variation of the Cu concentration, so that the sample containing 0.02 mmol of Cu dopant has the lowest PL intensity which implies promotion of the non-radiative decay of the excited electrons for this sample. For charge carriers to be effectively separated, the space charge layer thickness must be equal to penetration depth of light into semiconductor. The thickness of space charge layer

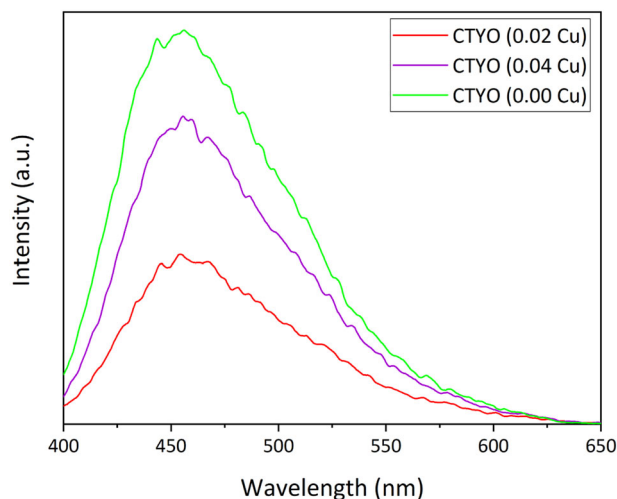


Fig. 6 PL spectra for the prepared CTYO with different concentrations of Cu dopant

gradually decreases with increasing the concentration of dopant. However, there is an optimum amount for dopant concentration, beyond this amount the thickness of space charge layer would be lower than the light penetration depth. As a result, the recombination rate of charge carriers would increase. Hence, the enhanced PL intensity at the more concentration of Cu dopant (0.04 mmol) is explained by the fact that the exceeded amount of dopant makes space charge layer narrower and leads to an increase in recombination rate of charges. Under this circumstance, photocatalyst material tends to emit light as a result of the enhanced recombination of charge carriers [3, 25].

3.2 Photocatalytic experiments for the prepared CTYO nanocomposite

The photocatalytic efficiency of the prepared CTYO nanocomposites with different concentrations of Cu dopant were evaluated for visible light degradation of AR88, as shown in Fig. 7a. As seen from DRS spectra, the 0.02 mmol Cu doped TiO_2/Yb_2O_3 nanocomposite has lower energy band gap and greater absorption in the range of visible light, so that the highest photocatalytic efficiency is belonged to the CTYO nanocomposite with 0.02 mmol of Cu dopant. After 180 min visible light irradiation, about 92.5% of AR88 solution was degraded over 0.02-CTYO. However, the photocatalytic degradation of AR88 solution is decreased over 0.04-CTYO which is truly attributed to the enhanced recombination of charges at the increased concentration of Cu dopant ($Cu = 0.04$ mmol). In addition, the photocatalytic degradation of AR88 was also studied under no light and without catalyst condition. As shown in Fig. 7a, the degradation of AR88 solution is negligible under both no light and without CTYO photocatalyst. For comparison,

Fig. 7 Photocatalytic activity (a) and Kinetic curves (b) for visible light degradation of AR88 using different CTYO photocatalyst

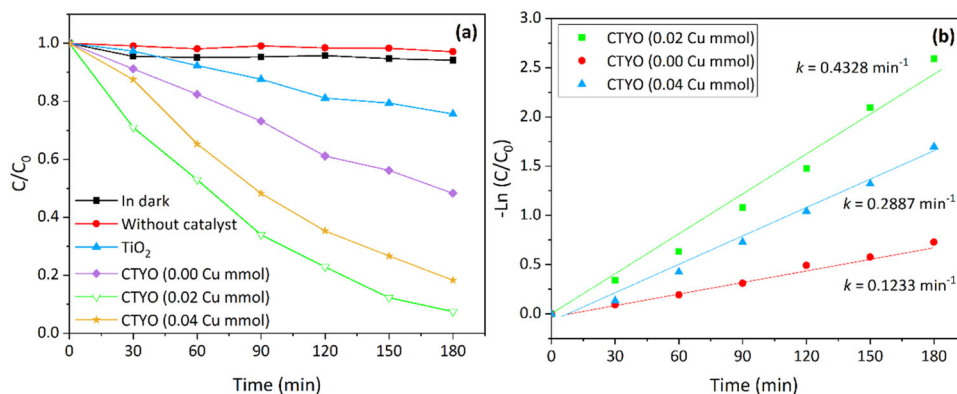
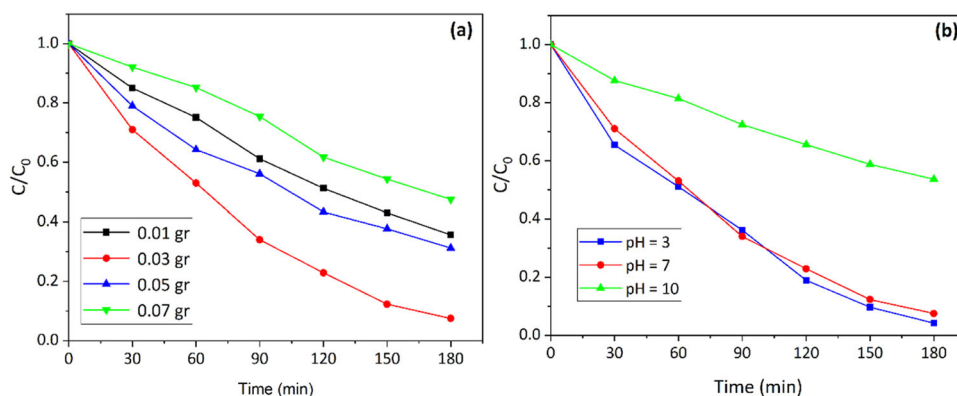


Fig. 8 Degradation of AR88 under different conditions. Photocatalyst amount (a) and pH solution (b)



degradation efficiency of AR88 over the prepared pure TiO_2 was provided which revealed inferior photocatalytic performance of the pure TiO_2 photocatalyst.

Figure 7b describes the kinetic of AR88 degradation over the different CTYO photocatalysts by plotting $-\ln(C/C_0)$ vs. irradiation time. As can be seen from Fig. 7b, the photocatalytic reaction using the prepared CTYO photocatalyst obeys from first order reaction kinetic ($-\ln C/C_0=kt$), where k is the rate constant of reaction (min^{-1}), t is the visible irradiation time, C_0 and C are initial and final concentration of AR88 solution, respectively. It is clear that the highest reaction rate (0.4328 min^{-1}) is belonged to the 0.02 mmol Cu doped TiO_2/Yb_2O_3 photocatalyst.

The photocatalytic activity of the prepared 0.02-CTYO photocatalyst was studied under different conditions. Figure 8a shows the photocatalytic degradation of AR88 solution in 4 separate reactions including different amounts of added photocatalyst. As clearly seen from Fig. 8a, the photocatalytic degradation of AR88 solution is dramatically decreased with increasing the amount of added photocatalyst material into reaction media. This observation could be attributed to the decreased penetration of light beam into reaction zone which is due to the enhanced turbidity of dye solution at the exceeded amount of loaded photocatalyst material [26, 27]. By comparison of the photocatalytic degradation efficiency for different amounts

of loaded photocatalyst, it was found that the optimum amount of CTYO photocatalyst is 0.03 g, so that 92.5% of the AR88 was degraded after 180 min visible light irradiation.

In addition, the photocatalytic experiments were conducted under different pH of AR88 solution (pH = 3, 7 and 10) using constant amount of the photocatalyst (0.03 g), as shown in Fig. 8b. In contrast to the basic condition (pH = 10), the photocatalytic efficiency of the prepared 0.02-CTYO photocatalyst is high at the acidic pH of AR88 solution (pH = 3). This observation is described by the fact that at the acidic pH of AR88 solution, the surface of photocatalyst particles is positively charged, whereas under higher pH (pH = 10) the photocatalyst particles have the negative surface charges. Since the positively charged surface increasingly prompts the adsorption of AR88 molecules on the surface of photocatalyst particles, the photocatalytic efficiency is high under acidic condition [28, 29].

The stability and efficiency of the prepared 0.02-CTYO photocatalyst were studied in the more photocatalytic reactions. Figure 9 describes the photocatalytic degradation of AR88 solution at the 8 successive reaction cycles. After each reaction cycle, the photocatalyst particles were separated from reaction media using centrifugation at 6000 rpm for 10 min. The collected photocatalyst material was washed using distilled water and ethanol to remove the

remaining dye molecules from the surface of the photocatalyst material and then was dried at 90 °C for 60 min.

As seen from Fig. 9, the stability and recyclability of the CTYO photocatalyst is high even after 8 successive reaction cycles. The loss of photocatalytic efficiency is only about

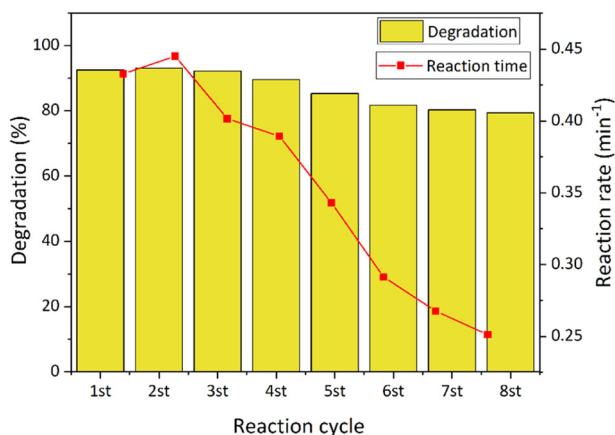


Fig. 9 Recyclability experiment for the prepared CTYO photocatalyst

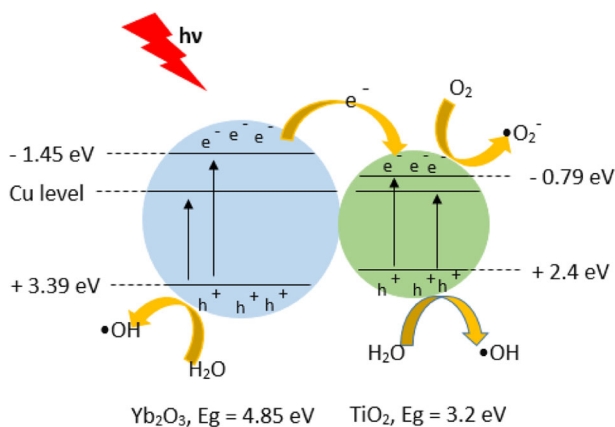


Fig. 10 Proposed mechanism for degradation of AR88 using CTYO nanocomposite

3% after 4 reaction cycles. However, the efficiency of the CTYO photocatalyst for degradation of AR88 solution was further reduced to 13.14% after 8 reaction cycles.

In addition, Fig. 9 shows the variation in the photocatalytic reaction rate during 8 successive reaction cycles. Obviously, the photocatalytic reaction rate for degradation of AR88 significantly decreases after 4 times reuses of the CTYO photocatalyst.

3.3 Mechanism of photocatalytic reaction over CTYO nanocomposite

Figure 10 shows the proposed mechanism for describing the photoactivity of CTYO nanocomposite. As shown, TiO₂ has the more anodic conduction band compared to the corresponding band in Yb₂O₃ which derives the photo-generated electrons toward CB of TiO₂. On the other hand, the photo-generated holes remain in the valence band of Yb₂O₃ phase which is due to the more cathodic nature of valence band of Yb₂O₃ than that of TiO₂. The CuO dopants form a new energy level can act as carrier-trapping centers for the excited electrons which effectively promotes the separation of the charges. Moreover, the existence of CuO impurities has significant effects on the improvement of visible light sensitization of the prepared photocatalyst and reduction of the band gap for both TiO₂ and Yb₂O₃. Furthermore, dye molecules are degraded by highly reactive superoxides ($\bullet\text{O}_2^-$) and hydroxyls ($\bullet\text{OH}$) radicals which are produced via redox reactions occurred between adsorbed species and photo-generated electrons and holes.

The visible light photocatalytic activity of the prepared CTYO photocatalyst was compared against the previously reported mixed metal oxide based photocatalysts in literature. Table 1 summarizes the efficiency and some experimental conditions of reported mixed metal oxide photocatalyst materials. As observed, the prepared CTYO photocatalyst has the great and satisfying photocatalytic efficiency, which is comparable to the previously reported photocatalyst materials.

Table 1 Comparison between the prepared CTYO and previously reported mixed metal oxide based photocatalyst materials

Photocatalyst	Target	Degradation (%)	Time (min)	Light	Lamp	Power (W)	Distance (cm)	Ref.
0.02 Cu doped TiO ₂ /Yb ₂ O ₃	AR88	92.5	180	Visible	Osram	400	30	This work
TiO ₂ /Eu ₂ O ₃ /Gr	4-chlorophenol	88	280	Visible	Tungsten Xenon	300	6	[30]
TiO ₂ /CeO ₂	2,4-dichlorophenol	49	360	Visible	SF300B	33	Not reported	[22]
TiO ₂ /CeO ₂ /g-C ₃ N ₄	MB	97	180	Visible	Xenon	500	Not reported	[31]
ZnO/CeO ₂	MO-MB-phenol	95.9 - 97.4 - 96.2	150	Visible	Halogen Projection Lamp	250	Not reported	[32]
ZnO/CeO ₂ /Yb ₂ O ₃	Mo-CR-RhB-SF	80 - 78 - 73 - 68	40	sunlight	–	–	–	[17]
ZnO-Yb ₂ O ₃ -Pr ₂ O ₃	MB	99.8	60	sunlight	–	–	–	[33]
ZnO/Sm ₂ O ₃ /Y ₂ O ₃	MB	98.5	75	sunlight	–	–	–	[34]

4 Conclusions

In summary, we have prepared the CTYO nanocomposite via sol-gel method. The XRD results confirmed the existence of both TiO_2 and Yb_2O_3 in the structure of the prepared sample. The effect of different concentrations of Cu dopant were studied on the structural, optical and photocatalytic properties of CTYO nanoparticles. It was found that the optimum concentration of Cu dopant for achieving the highest visible light photoactivity was 0.02 mmol. The photocatalytic experiment was performed for the visible light degradation of AR88. The effect of different amounts of the loaded photocatalyst and different pH of AR88 solution were investigated on the degradation efficiency of AR88. Under recyclability experiments revealed that the prepared CTYO photocatalyst has the great stability toward visible light degradation of the AR88 solution.

Acknowledgements The author would like to acknowledge the financial support of this work by the Payame Noor University, Tehran, Iran.

Compliance with ethical standards

Conflict of interest The authors declare no competing interests.

References

- Schneider J, Matsuoka M, Takeuchi M, Zhang J, Horiuchi Y, Anpo M, Bahnemann DW (2014) Understanding TiO_2 Photocatalysis: Mechanisms and Materials. *Chem Rev* 114(19):9919–9986. <https://doi.org/10.1021/cr5001892>
- Zulfiqar M, Sufian S, Bahadar A, Lashari N, Rabat NE, Mansor N (2021) Surface-fluorination of TiO_2 photocatalysts for remediation of water pollution: A review. *J Clean Prod* 317:128354. <https://doi.org/10.1016/j.jclepro.2021.128354>
- Rahbar M, Mehrzad M, Behpour M, Mohammadi-Aghdam S, Ashrafi M (2019) S, N co-doped carbon quantum dots/ TiO_2 nanocomposite as highly efficient visible light photocatalyst. *Nanotechnology* 30(50):505702. <https://doi.org/10.1088/1361-6528/ab40dc>
- Zhang Y, Sun A, Xiong M, Macharia DK, Liu J, Chen Z, Li M, Zhang L (2021) TiO_2/BiOI p-n junction-decorated carbon fibers as weavable photocatalyst with UV–vis photoresponsive for efficiently degrading various pollutants. *Chem Eng J* 415:129019. <https://doi.org/10.1016/j.cej.2021.129019>
- Fawzi Suleiman Khasawneh O, Palaniandy P (2021) Removal of organic pollutants from water by $\text{Fe}_2\text{O}_3/\text{TiO}_2$ based photocatalytic degradation: A review. *Environ Technol Innov* 21:101230. <https://doi.org/10.1016/j.eti.2020.101230>
- Pelaez M, Nolan NT, Pillai SC, Seery MK, Falaras P, Kontos AG, Dunlop PSM, Hamilton JWJ, Byrne JA, O'Shea K, Entezari MH, Dionysiou DD (2012) A review on the visible light active titanium dioxide photocatalysts for environmental applications. *Appl Catal B: Environ* 125:331–349. <https://doi.org/10.1016/j.apcatb.2012.05.036>
- Daghrir R, Drogui P, Robert D (2013) Modified TiO_2 For Environmental Photocatalytic Applications: A Review. *Ind Eng Chem Res* 52(10):3581–3599. <https://doi.org/10.1021/ie303468t>
- Rahbar M, Behpour M (2022) Fluorite type $\text{La}_2\text{Pb}_2\text{O}_7$ nanoparticles coated onto AgO as enhanced performance cathode active material for alkaline primary cell. *J Power Sources* 521:230887
- Delbari SA, Ghadimi LS, Hadi R, Farhoudian S, Nedaei M, Babapoor A, Namini AS, Van Le Q, Shokouhimehr M, Asl MS (2021) Transition metal oxide-based electrode materials for flexible supercapacitors: A review. *J Alloy Compd* 857:158281
- Salih EY, Sabri MFM, Eisa MH, Sulaiman K, Ramizy A, Hussein MZ, Said SM (2021) Mesoporous $\text{ZnO}/\text{ZnAl}_2\text{O}_4$ mixed metal oxide-based Zn/Al layered double hydroxide as an effective anode material for visible light photodetector. *Mater Sci Semiconduct Proc* 121:105370
- Teh CM, Mohamed AR (2011) Roles of titanium dioxide and ion-doped titanium dioxide on photocatalytic degradation of organic pollutants (phenolic compounds and dyes) in aqueous solutions: A review. *J Alloy Compd* 509(5):1648–1660
- Štengl V, Bakardjieva S, Murafa N (2009) Preparation and photocatalytic activity of rare earth doped TiO_2 nanoparticles. *Mater Chem Phys* 114(1):217–226
- Janani FZ, Khair H, Taoufik N, Elhalil A, Sadiq M, Puga AV, Mansouri S, Barka N (2021) $\text{ZnO}-\text{Al}_2\text{O}_3-\text{CeO}_2-\text{Ce}_2\text{O}_3$ mixed metal oxides as a promising photocatalyst for methyl orange photocatalytic degradation. *Mater Today Chem* 21:100495. <https://doi.org/10.1016/j.mtchem.2021.100495>
- Vignesh S, Suganthi S, Palanivel B, Ali AM, Shkir M, Algarni H, Sreedevi G (2022) Design a novel g-C $_3$ N $_4$ based $\text{Ce}_2\text{O}_3/\text{CuO}$ ternary photocatalysts for superior photo-degradation performance of organic mixed pollutants: Insights of Z-scheme charge transfer mechanism. *J Phys Chem Solids* 162:110514. <https://doi.org/10.1016/j.jpcs.2021.110514>
- Mohamed RM, Ismail AA, Kadi MW, Alresheedi AS, Mkhallid IA (2021) Photocatalytic performance mesoporous Nd_2O_3 modified ZnO nanoparticles with enhanced degradation of tetracycline. *Catal Today* 380:259–267. <https://doi.org/10.1016/j.cattod.2020.11.002>
- Basaleh A, Ismail AA, Mohamed RM (2022) Novel visible light heterojunction $\text{CdS}/\text{Gd}_2\text{O}_3$ nanocomposites photocatalysts for Cr(VI) photoreduction. *J Alloy Compd* 927:166988. <https://doi.org/10.1016/j.jallcom.2022.166988>
- Munawar T, Mukhtar F, Nadeem MS, Riaz M, Naveed ur Rahman M, Mahmood K, Hasan M, Arshad MI, Hussain F, Hussain A, Iqbal F (2020) Novel photocatalyst and antibacterial agent; direct dual Z-scheme $\text{ZnO}-\text{CeO}_2-\text{Yb}_2\text{O}_3$ heterostructured nanocomposite. *Solid State Sci* 109:106446. <https://doi.org/10.1016/j.solidstasciences.2020.106446>
- Modwi A, Aissa B, Taha KK, Khezami L, El Ghoul J, Al-Ayed AS, Bououdina M (2021) Fabrication of $(\text{Y}_2\text{O}_3)_n-\text{ZnO}$ nanocomposites by high-energy milling as potential photocatalysts. *J Mater Sci: Mater Electron* 32(3):3415–3430
- Liyanaarachchi H, Thambiliyagodage C, Liyanaarachchi C, Samarakoon U (2023) Efficient photocatalysis of Cu doped $\text{TiO}_2/\text{g}-\text{C}_3\text{N}_4$ for the photodegradation of methylene blue. *Arab J Chem* 16(6):104749. <https://doi.org/10.1016/j.arabjc.2023.104749>
- Yuzer B, Aydın MI, Con AH, Inan H, Can S, Selcuk H, Kadmi Y (2022) Photocatalytic, self-cleaning and antibacterial properties of Cu(II) doped TiO_2 . *J Environ Manag* 302:114023. <https://doi.org/10.1016/j.jenvman.2021.114023>
- Shirazi P, Rahbar M, Behpour M, Ashrafi M (2020) $\text{La}_2\text{MnTiO}_6$ double perovskite nanostructures as highly efficient visible light photocatalysts. *N J Chem* 44(1):231–238
- Gnanasekaran L, Rajendran S, Priya AK, Durgalakshmi D, Vo D-VN, Comejo-Ponce L, Gracia F, Soto-Moscoco M (2021) Photocatalytic degradation of 2,4-dichlorophenol using bio-green assisted $\text{TiO}_2-\text{CeO}_2$ nanocomposite system. *Environ Res* 195:110852. <https://doi.org/10.1016/j.envres.2021.110852>

23. Colón G, Maicu M, Hidalgo MC, Navío JA (2006) Cu-doped TiO₂ systems with improved photocatalytic activity. *Appl Catal B: Environ* 67(1):41–51. <https://doi.org/10.1016/j.apcatb.2006.03.019>
24. Eskandarloo H, Badieli A, Behnajady MA (2014) TiO₂/CeO₂ hybrid photocatalyst with enhanced photocatalytic activity: optimization of synthesis variables. *Ind Eng Chem Res* 53(19):7847–7855
25. Yao Y, Li G, Ciston S, Lueptow RM, Gray KA (2008) Photo-reactive TiO₂/carbon nanotube composites: synthesis and reactivity. *Environ Sci Technol* 42(13):4952–4957
26. Anandan S, Kumar PS, Pugazhenthiran N, Madhavan J, Maruthamuthu P (2008) Effect of loaded silver nanoparticles on TiO₂ for photocatalytic degradation of Acid Red 88. *Sol Energy Mater Sol Cells* 92(8):929–937
27. Kumar PSS, Sivakumar R, Anandan S, Madhavan J, Maruthamuthu P, Ashokkumar M (2008) Photocatalytic degradation of Acid Red 88 using Au–TiO₂ nanoparticles in aqueous solutions. *Water Res* 42(19):4878–4884
28. Kartal ÖE, Erol M, Oğuz H (2001) Photocatalytic destruction of phenol by TiO₂ powders. *Chem Eng Technol: Ind Chem-Plant Equip-Process Eng-Biotechnol* 24(6):645–649
29. Van Doorslaer X, Demeestere K, Heynderickx PM, Van Langenhove H, Dewulf J (2011) UV-A and UV-C induced photolytic and photocatalytic degradation of aqueous ciprofloxacin and moxifloxacin: reaction kinetics and role of adsorption. *Appl Catal B: Environ* 101(3–4):540–547
30. Myilsamy M, Mahalakshmi M, Subha N, Rajabhuvaneswari A, Murugesan V (2016) Visible light responsive mesoporous graphene–Eu₂O₃/TiO₂ nanocomposites for the efficient photocatalytic degradation of 4-chlorophenol. *RSC Adv* 6(41):35024–35035. <https://doi.org/10.1039/C5RA27541E>
31. Vignesh S, Chandrasekaran S, Srinivasan M, Anbarasan R, Perumalsamy R, Arumugam E, Shkir M, Algarni H, AlFaify S (2022) TiO₂-CeO₂/g-C₃N₄ S-scheme heterostructure composite for enhanced photo-degradation and hydrogen evolution performance with combined experimental and DFT study. *Chemosphere* 288:132611. <https://doi.org/10.1016/j.chemosphere.2021.132611>
32. Rajendran S, Khan MM, Gracia F, Qin J, Gupta VK, Arumainathan S (2016) Ce³⁺-ion-induced visible-light photocatalytic degradation and electrochemical activity of ZnO/CeO₂ nanocomposite. *Sci Rep* 6(1):31641. <https://doi.org/10.1038/srep31641>
33. Munawar T, Yasmeen S, Hasan M, Mahmood K, Hussain A, Ali A, Arshad MI, Iqbal F (2020) Novel tri-phase heterostructured ZnO–Yb₂O₃–Pr₂O₃ nanocomposite; structural, optical, photocatalytic and antibacterial studies. *Ceram Int* 46(8, Part A):11101–11114. <https://doi.org/10.1016/j.ceramint.2020.01.130>
34. Munawar T, Mukhtar F, Nadeem MS, Mahmood K, Hussain A, Ali A, Arshad MI, Ajaz un Nabi M, Iqbal F (2020) Structural, optical, electrical, and morphological studies of rGO anchored direct dual-Z-scheme ZnO–Sm₂O₃–Y₂O₃ heterostructured nanocomposite: An efficient photocatalyst under sunlight. *Solid State Sci* 106:106307. <https://doi.org/10.1016/j.solidstatesciences.2020.106307>

Publisher's note Springer Nature remains neutral with regard to jurisdictional claims in published maps and institutional affiliations.

Springer Nature or its licensor (e.g. a society or other partner) holds exclusive rights to this article under a publishing agreement with the author(s) or other rightsholder(s); author self-archiving of the accepted manuscript version of this article is solely governed by the terms of such publishing agreement and applicable law.